At the crossroads of astrophysics and cosmology: Period–luminosity relations in the 2020s
Proceedings IAU Symposium No. 376, 2024
R. de Grijs, P. A. Whitelock & M. Catelan, eds.
doi:10.1017/S1743921323003319

Granulation in Red Supergiants: The Scaling Relations

Yi Ren[1], Zehao Zhang[2,3], Biwei Jiang[2,3], Igor Soszyński[4] and Tharindu Jayasinghe[5]

[1]College of Physics and Electronic Engineering, Qilu Normal University, Jinan 250200, China
email: yiren@qlnu.edu.cn

[2]Institute for Frontiers in Astronomy and Astrophysics, Beijing Normal University, Beijing 102206, China
email: bjiang@bnu.edu.cn

[3]Department of Astronomy, Beijing Normal University, Beijing 100875, China

[4]Astronomical Observatory, University of Warsaw, Al. Ujazdowskie 4, 00-478 Warszawa, Poland

[5]Department of Astronomy, University of California Berkeley, Berkeley CA 94720, USA
NASA Hubble Fellow

Abstract. The evolution of granulation is an important mechanism of the light variations of red supergiants (RSGs). Based on pure and complete samples of RSGs in the Magellanic Clouds, the mechanisms and characteristics of the granulation of RSGs are investigated based on time-series data. As predicted by the basic physical process of granulation and previous works, there are tight relations between granulation and stellar parameters of RSGs (i.e., the scaling relations). The scaling relations of RSGs provide a new method to infer stellar parameters by using the characteristic timescale and amplitude of granulations. Some faint sources deviate from the scaling relations, which may be due to the difference in the properties of the granulation of the RSGs before and after the blue loop or contamination by Mira variables. However, both of these possibilities suggest that the scaling relations of granulation is different among different types of stars.

Keywords. Red supergiant stars, Stellar pulsations, Stellar oscillations, Late-type stars

1. Introduction

Red supergiants (RSGs) are massive Population I stars in the core helium-burning stage. The initial mass of RSGs is generally considered to be between $7-30\,M_{\odot}$ (Yang *et al.* 2019; Ren *et al.* 2021a). They have relatively low effective temperatures, from $\sim 3000-4500$ K. The radii of RSGs can reach $\sim 1500\,R_{\odot}$. Hence, RSGs have the high luminosity of $3500-630{,}000\,L_{\odot}$ and low surface gravity.

RSGs exhibit various types of light variability; according to the characteristics of the light curves, the variations of RSGs are usually divided into three types: semi-regular variation, irregular variation, and variation with a long secondary period (LSP). Unfortunately, the mechanism producing LSPs remains unclear. The semi-regular variation exhibits the period-luminosity relations (PLR) theoretically and observationally (Guo & Li 2002; Kiss *et al.* 2006; Yang & Jiang 2011, 2012; Soraisam *et al.* 2018; Ren *et al.* 2019); this PLR makes RSGs a potential standard candle. In the case of irregular variations, the red noise ($1/f$ noise) found in the power spectra suggests that they

are relates to stochastic mechanisms (i.e., granulation; Kiss *et al.* 2006; Yang & Jiang 2008). Three-dimensional radiative hydrodynamics (RHD) simulations and interferometric observations of Betelgeuse also proved that there are granulations on its surface (Chiavassa *et al.* 2009, 2010). However, direct imaging observation for distant RSGs is not possible, Betelgeuse is the only case for investigating the granulations of RSGs.

Using the time-series data from the All-Sky Automated Survey for SuperNovae (ASAS-SN; Shappee *et al.* 2014; Kochanek *et al.* 2017; Jayasinghe *et al.* 2020) and the intermediate Palomar Transient Factory (iPTF; Law *et al.* 2009; Rau *et al.* 2009) survey, and the sample of RSGs from Massey & Evans (2016), Yang *et al.* (2018, 2019), Ren *et al.* (2019), and Ren & Jiang (2020) investigated light variations of RSGs in the Small Magellanic Cloud (SMC), Large Magellanic Cloud (LMC), and M31, and determined the characteristic timescale and amplitude of granulations. They found tight relations (i.e., the scaling relations) between granulation parameters (timescale and amplitude) and stellar parameters (luminosity, mass, surface gravity, radius, effective temperature), which are in agreement with predictions from the basic physical process. They also compared their RSGs with red giant branch (RGB) stars and Betelgeuse. It is found that the relations fall close to the extrapolated relations followed by RGB stars. These results illustrate that the granulations constitute an important mechanism that contributes to the light variation of RSGs.

Moreover, for RSGs, the scaling relations provide a new method to infer stellar parameters using time-series data. This is very meaningful for the measurement of mass and surface gravity because there are few methods to determine the mass and surface gravity of RSGs. Therefore, we need more complete samples and time-series data to test whether the scaling relations are applicable to all RSGs. Using astrometric information from *Gaia* (Gaia Collaboration *et al.* 2018) and near-infrared photometry from the Two Micron All Sky Survey (2MASS; Skrutskie *et al.* 2006), Yang *et al.* (2020, 2021) and Ren *et al.* (2021b) removed foreground contaminations and established the most pure and complete samples of RSGs in the SMC and LMC. Based on the samples of RSGs and time-series data from the Optical Gravitational Lensing Experiment (OGLE; Udalski *et al.* 2015; Soszyński *et al.* 2015) and ASAS-SN, this work systematically investigates the scaling relations of RSGs.

2. Dynamic Properties of Granulations in Red Supergiants

The granulations in most of the RSGs evolve at an effective timescale ($\tau_{\rm eff}$) of several days to one year, with a characteristic amplitude ($\sigma_{\rm gran}$) of $10-1000$ mmag (Ren & Jiang 2020). $\tau_{\rm eff}$ and $\sigma_{\rm gran}$ are found to increase with metallicity, which may indicate the influence of metallicity on the granulation characteristics.

The most important dynamic property of granulations is the relation between granulation and stellar parameters, namely the scaling relation. Figure 1 presents the scaling relation of RSGs derived by Ren & Jiang (2020). RGB stars and some well-known stars (Betelgeuse, V1154 Cyg, the Sun) are included for comparison. Betelgeuse is an RSG, V1154 Cyg is a classical Cepheid, and the Sun is a G-type main-sequence star (G2V). In Figure 1, different types of stars almost follow the same scaling relation. Although RGB stars are offset towards smaller $\tau_{\rm eff}$ than suggested by the proposed scaling relation, it may be caused by different granulation parameters measurement methods. We can speculate that the scaling relation is applicable to all stars with granulations. If the scaling relation is universal for stars with granulations, then it would be a universal method for inferring stellar parameters that could be widely used.

In this work, we use the most complete and pure samples of RSGs to analyze the scaling relations in detail.

https://doi.org/10.1017/S1743921323003319 Published online by Cambridge University Press

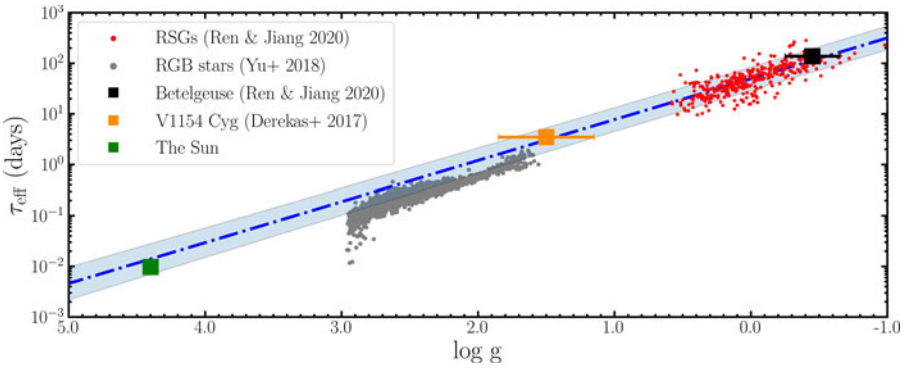

Figure 1. Relation of the granulation effective timescale $\tau_{\rm eff}$ with $\log g$. The results for RSGs (red dots) are taken from Ren & Jiang (2020), RGB stars (gray dots) are taken from Yu *et al.* (2018) and de Assis Peralta *et al.* (2018), V1154 Cyg (orange square) is taken from Derekas *et al.* (2017), and Betelgeuse (black square) is taken from Derekas *et al.* (2017) and Ren & Jiang (2020). The timescale of granulations in the Sun (green square) is $8-20$ minutes; we take the average value of 14 minutes in this figure. The blue dash-dotted line is the robust linear fit with the 95% confidence region (blue shaded region) based on RSGs.

3. Time-Series Data

ASAS-SN consists of 20 telescopes all around the globe that observed variable objects in the SMC and LMC at a cadence of $1-2$ days over a period time spanning ~ 2000 days. The magnitude limits are ~ 18 in the g band and ~ 17 in the V band. OGLE is a long-term photometric survey focused on variables, the brightness of sources in the SMC and LMC is sampled at a cadence of $4-8$ days, and OGLE has accumulated time-series data over 10 years (see Table 1).

Figure 2 shows the collections of g, V, and I-band light curves of two RSGs in the LMC. Figure 3 plots the 2MASS/K_0 distributions of sources along with ASAS-SN V-band and OGLE-IV I-band light curves, where K_0 are extinction corrected using reddening maps of MCs (Skowron *et al.* 2021). ASAS-SN mainly observes brighter sources, while OGLE mainly observes fainter sources.

3.1. *Time-Series Data Processing*

In order to exclude the influence of outliers in photometry on further analysis, we first calculate the first quartile (Q_1), the third quartile (Q_3), and the corresponding interquartile range (IQR; $\mathrm{IQR} = Q_3 - Q_1$) according to the distribution of magnitudes for each light curve, and then the photometry points smaller than $Q_1 - 1.5 \times \mathrm{IQR}$ or larger than $Q_3 + 1.5 \times \mathrm{IQR}$ are removed from the light curve.

In this work, for ASAS-SN images, we perform forced photometry at the coordinates of the RSGs. Though the brightness of some faint sources is fainter than the detection threshold, ASAS-SN still generates a light curve. In addition, the amplitudes of granulations of some faint RSGs are relatively small. When observing at a longer wavelength (i.e., in the I band), their amplitudes will be even smaller. Therefore, it may be difficult to detect the signal of granulations in the light curves of some faint sources. In order to solve both these problems, we conduct a white noise test on the light curves. If the light curves are determined to be a white noise sequence, they are excluded from further analysis. Specifically, the autocorrelation functions (ACFs) of a light curve are calculated at 50 time lags. If less than 5% of the thus-computed ACFs meet the condition $|\mathrm{ACFs}| < 1.96/\sqrt{n}$ (where n is the length of the time-series data), we accept the

https://doi.org/10.1017/S1743921323003319 Published online by Cambridge University Press

Table 1. Number of Light Curves.

Galaxy	*g* band	*V* band	*I* band	At least one band	Containing *gVI* bands
SMC	886	452	1337	1924	83
LMC	2665	2123	2656	4471	451

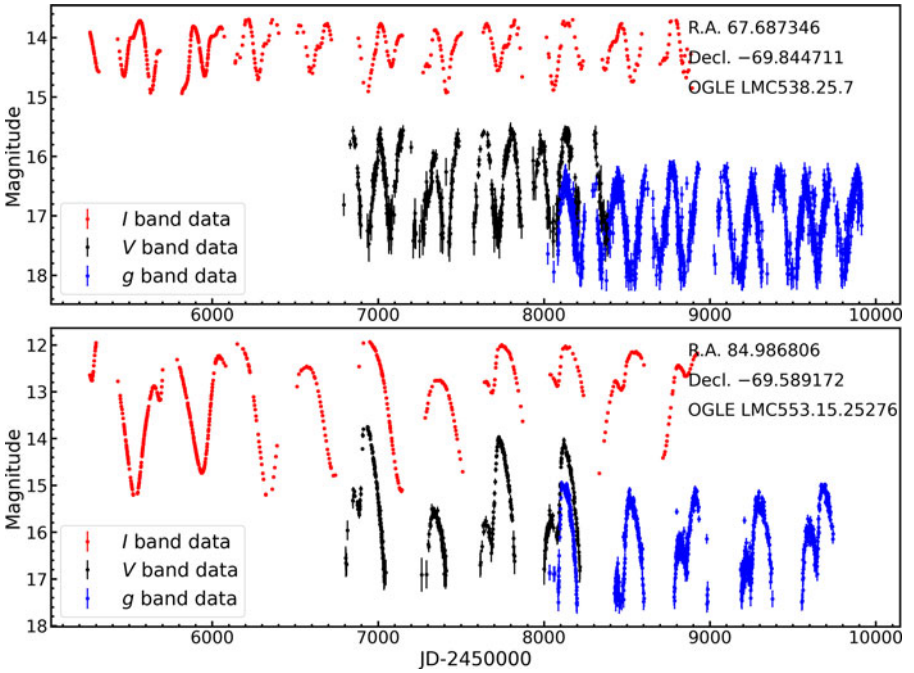

Figure 2. Examples of light curves of RSGs in the LMC after removing outliers. The ASAS-SN *V* and *g* band time-series data are shown in black and blue dots with error bars, respectively. *I*-band photometry is taken from OGLE-IV and is presented as red dots with error bars.

hypothesis that the time-series data constitutes a white noise sequence. Figure 4 gives an example of how we identify a white-noise process.

4. Granulation Parameters

Harvey (1985) proposed a famous model to describe the dynamic properties of granulations. The granulation evolution over time can be modeled as a stochastic process with an exponential decay ACF and variance $\sigma^2_{\rm gran}$. This model leads to a Lorentz profile power spectrum (hereafter Harvey function):

$$P(\nu) = \frac{4\sigma^2_{\rm gran}\tau_{\rm gran}}{1 + (2\pi\nu\tau_{\rm gran})^2}, \quad (1)$$

in which $P(\nu)$ is the total power at frequency ν. The key parameters in Equation 1 are the characteristic timescale $\tau_{\rm gran}$ and characteristic amplitude $\sigma_{\rm gran}$. $\tau_{\rm gran}$ and $\sigma_{\rm gran}$ can thus be determined by fitting the power spectral density (PSD) using a Harvey-like function.

Ren & Jiang (2020) used the Continuous-time Auto Regressive Moving Average (CARMA) model (Kelly *et al.* 2014) to calculate the posterior PSDs of the light curves. Since the CARMA model is not affected by the noise of measurement, the Harvey-like

https://doi.org/10.1017/S1743921323003319 Published online by Cambridge University Press

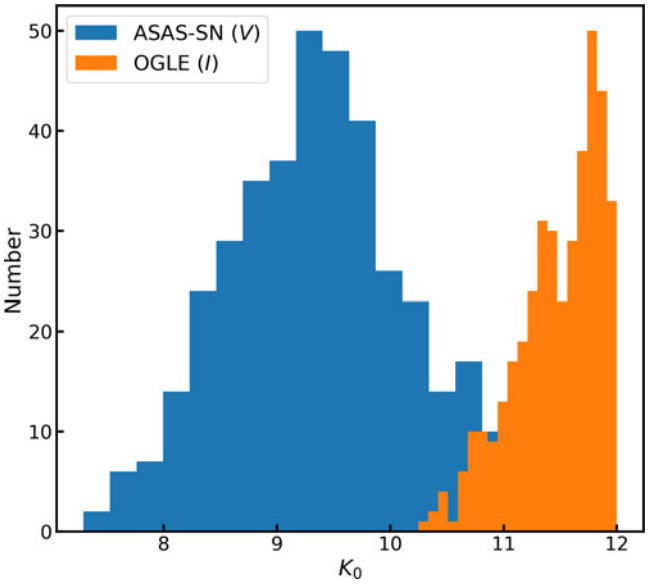

Figure 3. K_0 distributions of sources with ASAS-SN V-band light curves (blue histogram) and OGLE I-band light curves (orange histogram).

function is used to fit the posterior PSD. The Harvey-like function is the following:

$$P(\nu) = \frac{\xi \sigma_{\rm gran}^2 \tau_{\rm gran}}{1 + (2\pi\nu\tau_{\rm gran})^{\alpha}}, \tag{2}$$

where ξ is a normalization factor related to α as

$$\xi = 2\alpha \sin(\pi/\alpha). \tag{3}$$

In this work, the PSD of a light curve is calculated using the Lomb-Scargle (LS) periodogram (Lomb 1976; Scargle 1982), as shown in Figure 5.

At the high-frequency end, the PSD approaches the measurement noise, so the Harvey-like function with white noise term is selected to fit the PSD,

$$P(\nu) = W + \frac{4\sigma^2 \tau_{\rm gran}}{1 + (2\pi\nu\tau_{\rm gran})^{\alpha}}, \tag{4}$$

where W represents the white noise component in the PSD. As shown in Figure 5, a total PSD consists of a granulation component and a white noise component. The granulation parameters are derived from the granulation component.

In order to compare the characteristic timescales resulting from different α values, the effective timescale $\tau_{\rm eff}$ is introduced (Mathur *et al.* 2011). The ACF is the inverse Fourier transform of the PSD and is calculated from the latter numerically. Then $\tau_{\rm eff}$ is the required time for the ACF to get reduced to $1/e$ of its initial value.

5. The Scaling Relations

Table 2 lists the methods for obtaining stellar parameters used in the scaling relations. For RSGs, there is no better way to obtain the mass and surface gravity. The M and $\log g$ are taken from the empirical mass-luminosity relation (Stothers & Leung 1971).

Using the measured granulation and stellar parameters of RSGs in the LMC, the obtained scaling relations are presented in Figure 6. The green points in Figure 6 use the light curves in the V band. Since the amplitudes of granulations are different in the V

https://doi.org/10.1017/S1743921323003319 Published online by Cambridge University Press

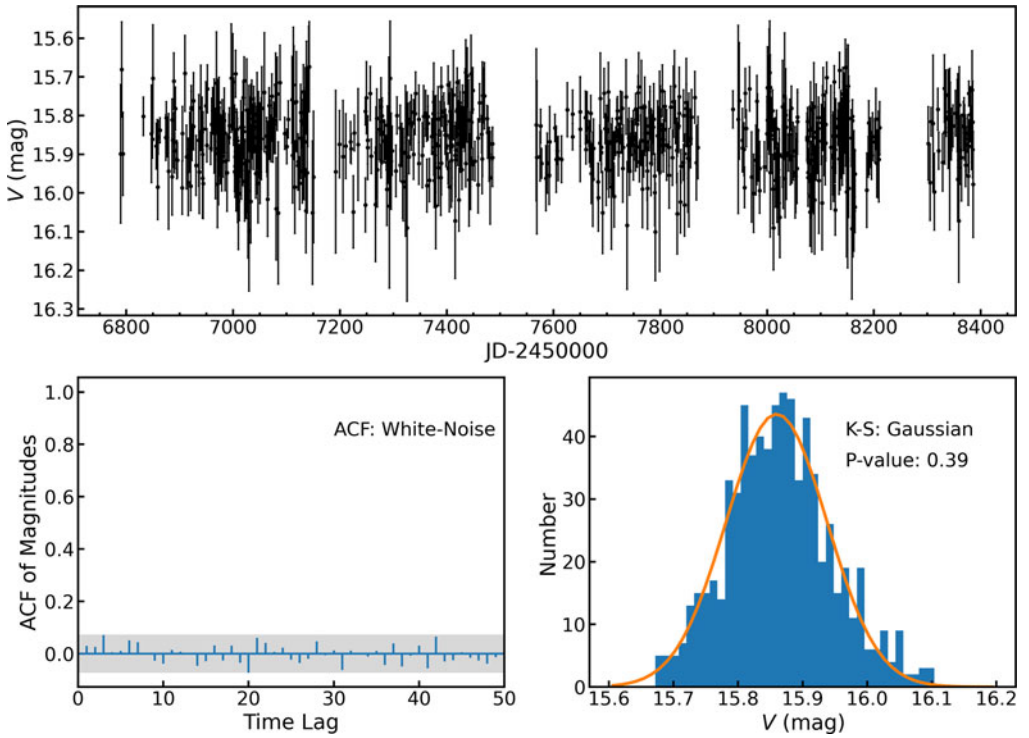

Figure 4. The upper panel shows an example of a light curve from ASAS-SN. This light curve constitutes a white noise sequence. The lower left panel indicates all the ACFs lay in the region assuming a white-noise process. In addition, we set up a null hypothesis that the distribution of brightness from the light curve obeys the normal distribution. Then a Kolmogorov-Smirnov (K-S) test is performed on the light curve, yielding a p-value of 0.39, which is greater than 0.05 (standard significance level). The p-value means we cannot reject the null hypothesis that the distribution of brightness from the light curve obeys the normal distribution (lower right panel). This confirms that the light curve is a Gaussian white noise sequence, which is thus excluded from further analysis.

and I bands, we multiply the amplitude in the I band by a factor of 1.231† to convert to the V-band amplitude for further analysis.

Compared to previous work (Ren & Jiang 2020), the scaling relations obtained include a group of fainter RSGs, which means that the sample covers a wider parameter space.

Most RSGs follow the scaling relations well ($\tau_{\rm eff}$ or $\sigma_{\rm gran}$ vs. L, $\log g$, M, etc). Figure 6 only displays the scaling relation between granulation parameters and $\log g$.

5.1. *Peculiar Sources*

As shown by the open circles in Figure 6, we note that some sources ("peculiar" sources) significantly deviate from the scaling relations. We speculate that there may be three possible reasons for these sources to deviate from the scaling relation.

(1) The light curves of these sources are rechecked, and it is found that some of them have relatively large amplitudes ($\Delta V > 0.3$ mag). Therefore, it is possible that the pulsating signal with large amplitude makes the measured granulation parameters larger. This is a technical explanation.

† The 29 RSGs in the LMC and 8 RSGs in the SMC have both I-band and V-band light curves. By fitting the granulation amplitudes $\sigma_{\rm gran}$ in these bands, we get $\sigma^{V}_{\rm gran} = 1.231\sigma^{I}_{\rm gran} + 0.006$. Thus, the amplitude ratio between the V and I band is 1.231.

https://doi.org/10.1017/S1743921323003319 Published online by Cambridge University Press

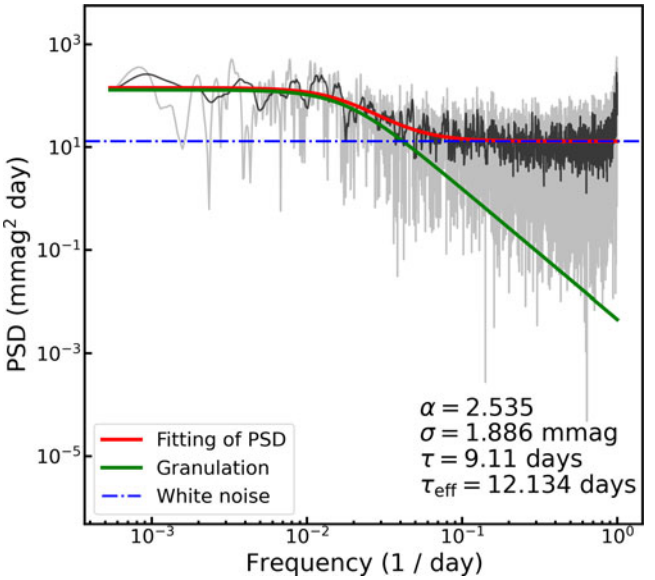

Figure 5. An example of fitting PSD using the Harvey-like function with white noise term. The gray line shows the PSD given by the LS algorithm, while the black line is the result of smoothing the gray line. The green solid line and blue dash-dotted line are the granulation component and measurement noise component, respectively.

(2) Another explanation is entirely physical. Some of these sources have very high light variation amplitudes ($\Delta V \sim 2$ mag), and their light variation characteristics are similar to those of Mira variables. Therefore, large-scale stellar phenomena may affect the dynamic properties of surface granulations.
(3) After calculating the mass of these sources, it is found that almost all sources with mass greater than 12 $M_\odot$ obey the scaling relations, while sources with mass less than 12 $M_\odot$ are divided into two groups. By comparing with Padova stellar evolution models (Chen *et al.* 2015; Pastorelli *et al.* 2020), it is found that an RSG with mass less than 12 $M_\odot$ will experience a blue loop, while an RSG with mass greater than 12 $M_\odot$ will not experience a blue loop. Therefore, the sources with less than 12 $M_\odot$ are divided into two groups, one of which represents the RSGs before the blue loop stage which follow the main branch, while the other group represents the RSGs after the blue loop stage which deviate from the main branch (minor branch).

The above three possibilities will be explored in a future paper through the stellar evolution model or data simulation method.

5.2. *Inferring Stellar Parameters Using the Scaling Relations*

The scaling relations provide a new method for inferring the stellar parameters of RSGs. In order to estimate the accuracy of this method, we perform linear fits (removing peculiar sources by eye-check) by taking granulation parameters as independent variables and the stellar parameters as dependent variables. The fitting form is as follows:

$$\log Y = k \times \log X + b, \tag{5}$$

where Y is one of g, $M/M_\odot$, $R/R\odot$, $L/L_\odot$, and $T_{\rm eff}$, and X is either $\tau_{\rm eff}$ or $\sigma_{\rm gran}$. Then an unbiased estimator, $\hat{\sigma}^{*2} = S_E^2/(n-2)$, where S_E is the residual sum of squares, is introduced to express the uncertainty of stellar parameters inferred by scaling relations.

https://doi.org/10.1017/S1743921323003319 Published online by Cambridge University Press

Table 2. Methods for Obtaining Stellar Parameters.

Stellar Parameter	Method	Reference
$T_{\rm eff}$	$T_{\rm eff}$ – $(J-K)_0$ relation^{*a}	—
L	$\log(L/L_\odot) = a + b\,(m_K - \mu)^{*b}$	Davies *et al.* (2013)
M	$(M/M_\odot)^\gamma = L/L_\odot$, $\gamma = 4$	Stothers & Leung (1971)
R	$R = (4\pi\sigma)^{-0.5} L^{0.5} T_{\rm eff}^{-2}$	—
g	$g = GM/R^2$	—

^{*a}The $T_{\rm eff}$ – $(J-K)_0$ relation is obtained by performing linear fitting between $(J-K)_0$ from Ren *et al.* (2021b) and $T_{\rm eff}$ from APOGEE (Abdurro'uf *et al.* 2022).

$^{*b}a = 0.90$, $b = -0.40$, $\mu = 18.72$ (18.26) for SMC (LMC).

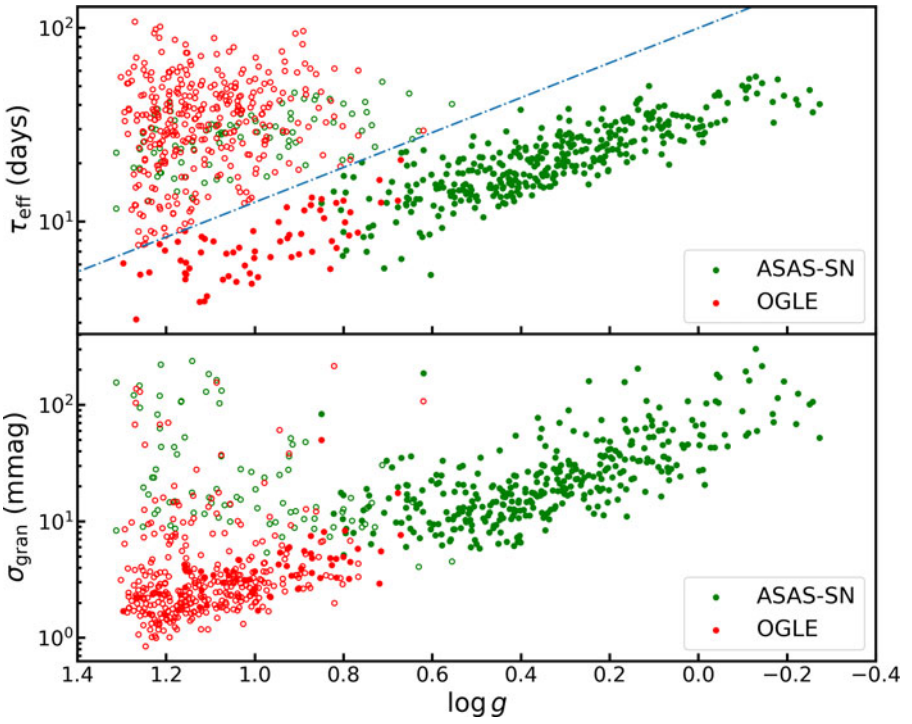

Figure 6. The scaling relation between effective timescale ($\tau_{\rm eff}$) and $\log g$ (top panel) and between granulation amplitude ($\sigma_{\rm gran}$) and $\log g$ (bottom panel) for RSGs in the LMC. Green and red dots represent RSGs, whose light curves are taken from ASAS-SN and OGLE, respectively. The blue dash-dotted line distinguishes between sources that follow the scaling relation and sources that deviate from the scaling relation. The open circles are sources that deviate from the $\tau_{\rm eff} - \log g$ relation.

$\hat{\sigma}^{*2}$ values of the fitting residuals of the scaling relations between five different stellar parameters and two granulation parameters are listed in Table 3.

As shown in Table 3, the scaling relations do indeed provide an accurate method to infer stellar parameters. For example, using the $\tau_{\rm eff} - \log g$ relation, the 1σ uncertainty in $\log g$ is 0.14.

6. Summary

Ren & Jiang (2020) proposed a method to measure the granulation parameters of RSGs using light curves and derived the scaling relations between granulation and stellar parameters for RSGs for the first time. They proved that the surfaces of RSGs are dominated by a few but huge granules, and that the evolution of granulations is an

https://doi.org/10.1017/S1743921323003319 Published online by Cambridge University Press

Table 3. Uncertainty of Stellar Parameters Inferred by Scaling Relations.

Stellar Parameter	$\hat{\sigma}^{*2}$, stellar parameters from $\tau_{\rm eff}$	$\hat{\sigma}^{*2}$, stellar parameters from $\sigma_{\rm gran}$
$\log g$	0.14	0.18
$\log(M/M_{\odot})$	0.04	0.06
$\log(R/R_{\odot})$	0.09	0.12
$\log(L/L_{\odot})$	0.17	0.22
$\log T_{\rm eff}$	0.01	0.01

important mechanism for modulating the light variation of RSGs. More importantly, the scaling relations provide a potential method for inferring their stellar parameters.

To test the universality of the scaling relations for RSGs, we investigated those based on new samples of RSGs in the SMC and LMC and time-series data from ASAS-SN and OGLE. The scaling relations obtained in this work cover a more expansive stellar parameter space. Most RSGs follow the scaling relations. However, some sources deviate from the latter. These sources generally have a large amplitude of light variation. The possible reasons may be the impact of large amplitude pulsations on measurements of granulation parameters, the impact of large amplitude pulsations on the physical properties of granulations, or the existence of two groups of sources corresponding to RSGs in the pre- or post- blue loop stages.

After removing sources that deviate from the scaling relations, we estimate the uncertainty of stellar parameters that are inferred from them. Excitingly, the scaling relations provide accurate inference of stellar parameters for RSGs.

Acknowledgements. This work is supported by the National Natural Science Foundation of China (NSFC) through grant Nos. 12133002 and 12203025, and Shandong Provincial Natural Science Foundation through project ZR2022QA064.

References

Abdurro'uf, Accetta, K., Aerts, C., *et al.* 2022, *ApJS*, 259, 35
Chen, Y., Bressan, A., Girardi, L., *et al.* 2015, *MNRAS*, 452, 1068
Chiavassa, A., Haubois, X., Young, J. S., *et al.* 2010, *A&A*, 515, A12
Chiavassa, A., Plez, B., Josselin, E., & Freytag, B. 2009, *A&A*, 506, 1351
Davies, B., Kudritzki, R.-P., Plez, B., *et al.* 2013, *ApJ*, 767, 3
de Assis Peralta, R., Samadi, R., & Michel, E. 2018, *AN*, 339, 134
Derekas, A., Plachy, E., Molnár, L., *et al.* 2017, *MNRAS*, 464, 1553
Gaia Collaboration, Brown, A. G. A., Vallenari, A., *et al.* 2018, *A&A*, 616, A1
Guo, J. H., & Li, Y. 2002, *ApJ*, 565, 559
Harvey, J. 1985, in ESA Special Publication, Vol. 235, Future Missions in Solar, Heliospheric & Space Plasma Physics, ed. E. Rolfe & B. Battrick, 199
Jayasinghe, T., Stanek, K. Z., Kochanek, C. S., *et al.* 2020, *MNRAS*, 491, 13
Kelly, B. C., Becker, A. C., Sobolewska, M., Siemiginowska, A., & Uttley, P. 2014, *ApJ*, 788, 33
Kiss, L. L., Szabó, G. M., & Bedding, T. R. 2006, *MNRAS*, 372, 1721
Kochanek, C. S., Shappee, B. J., Stanek, K. Z., *et al.* 2017, *PASP*, 129, 104502
Law, N. M., Kulkarni, S. R., Dekany, R. G., *et al.* 2009, *PASP*, 121, 1395
Lomb, N. R. 1976, *Ap&SS*, 39, 447
Massey, P., & Evans, K. A. 2016, *ApJ*, 826, 224
Mathur, S., Hekker, S., Trampedach, R., *et al.* 2011, *ApJ*, 741, 119
Pastorelli, G., Marigo, P., Girardi, L., *et al.* 2020, *MNRAS*, 498, 3283
Rau, A., Kulkarni, S. R., Law, N. M., *et al.* 2009, *PASP*, 121, 1334
Ren, Y., Jiang, B., Yang, M., *et al.* 2021a, *ApJ*, 907, 18
Ren, Y., Jiang, B., Yang, M., Wang, T., & Ren, T. 2021b, *ApJ*, 923, 232
Ren, Y., & Jiang, B.-W. 2020, *ApJ*, 898, 24
Ren, Y., Jiang, B.-W., Yang, M., & Gao, J. 2019, *ApJS*, 241, 35
Scargle, J. D. 1982, *ApJ*, 263, 835

Shappee, B. J., Prieto, J. L., Grupe, D., *et al.* 2014, *ApJ*, 788, 48
Skrutskie, M. F., Cutri, R. M., Stiening, R., *et al.* 2006, *AJ*, 131, 1163
Skowron, D. M., Skowron, J., Udalski, A., *et al.* 2021, *ApJS*, 252, 23
Soraisam, M. D., Bildsten, L., Drout, M. R., *et al.* 2018, *ApJ*, 859, 73
Soszyński, I., Udalski, A., Szymański, M. K., *et al.* 2015, *AcA*, 65, 297
Stothers, R., & Leung, K. C. 1971, *A&A*, 10, 290
Udalski, A., Szymański, M. K., & Szymański, G. 2015, *AcA*, 65, 1
Yang, M., & Jiang, B. W. 2008, in The Art of Modeling Stars in the 21st Century, ed. L. Deng & K. L. Chan, Vol. 252, 267
Yang, M., & Jiang, B. W. 2011, *ApJ*, 727, 53
Yang, M., & Jiang, B. W. 2012, *ApJ*, 754, 35
Yang, M., Bonanos, A. Z., Jiang, B.-W., *et al.* 2018, *A&A*, 616, A175
Yang, M., Bonanos, A. Z., Jiang, B.-W., *et al.* 2019, *A&A*, 629, A91
Yang, M., Bonanos, A. Z., Jiang, B.-W., *et al.* 2020, *A&A*, 639, A116
Yang, M., Bonanos, A. Z., Jiang, B., *et al.* 2021, *A&A*, 646, A141
Yu, J., Huber, D., Bedding, T. R., *et al.* 2018, *ApJS*, 236, 42